Study of Xenon Binding in Cryptophane-A Using Laser-Induced NMR Polarization Enhancement

Michel Luhmer,[†] Boyd M. Goodson,[‡,§] Yi-Qiao Song,[‡,§,||] David D. Laws,[‡,§] Lana Kaiser,[‡,§] Michelle C. Cyrier,[‡] and Alexander Pines*[,‡,§]

Contribution from the Materials Sciences Division, Lawrence Berkeley National Laboratory, Berkeley, California 94720, Department of Chemistry, University of California, Berkeley, California 94720, and Laboratoire de Chimie Organique E.P., Université Libre de Bruxelles, CP 165/64, Av. F.D. Roosevelt 50, 1050 Bruxelles, Belgium

Received December 3, 1998. Revised Manuscript Received February 2, 1999

Abstract: In solution, spin-polarization transfer between laser-polarized xenon and the hydrogen nuclei of nearby molecules leads to signal enhancements in the resolved ^{1}H NMR spectrum, offering new opportunities for probing the chemical environment of xenon atoms. Following binding of laser-polarized xenon to molecules of cryptophane-A, selective enhancements of the ^{1}H NMR signals were observed. A theoretical framework for the interpretation of such experimental results is provided, and the spin polarization-induced nuclear Overhauser effects are shown to yield information about the molecular environment of xenon. The observed selective ^{1}H enhancements allowed xenon−proton internuclear distances to be estimated. These distances reveal structural characteristics of the complex, including the preferred molecular conformations adopted by cryptophane-A upon binding of xenon.

Introduction

Xenon is chemically inert, yet exhibits NMR parameters that are highly sensitive to its chemical environment. Considerable work has therefore capitalized on the utility of ^{129}Xe ($I = {}^1/_2$) as a magnetic resonance probe of molecules, materials, and biological systems.[1−6] Much of this work has utilized the highly sensitive chemical shift of ^{129}Xe in order to reveal properties of the xenon environment. Selective polarization transfer from ^{1}H to ^{129}Xe has also been used to investigate sites of xenon binding[7] and xenon preferential solvation.[8] Such experiments have the advantage of providing direct microscopic information regarding the xenon surroundings and should prove useful for the interpretation of experimental ^{129}Xe chemical shifts, but they rely on the weak intermolecular cross-relaxation between ^{129}Xe and nuclear spins in its environment. Furthermore, selective irradiation in complex ^{1}H spectra can be difficult to achieve, and 2D heteronuclear ^{1}H−^{129}Xe NOESY experiments would be enormously time-consuming.

Using optical pumping methods,[9−12] the nuclear spin polarization of ^{129}Xe can be increased by 4−5 orders of magnitude; "laser-polarized" ^{129}Xe provides significantly enhanced sensitivity for a variety of NMR and MRI experiments.[13−24] For

* Address correspondence to Alexander Pines, Department of Chemistry, University of California, Berkeley, CA 94720. Telephone: (510) 642-1220. Fax: (510) 486-5744. E-mail: pines@cchem.berkeley.edu.

[†] Chargé de Recherches du F.N.R.S.; Université Libre de Bruxelles, Brussels, Belgium.

[‡] Department of Chemistry, University of California, Berkeley.

[§] Materials Sciences Division, Lawrence Berkeley National Laboratory.

[||] Present address: Schlumberger-Doll Research, Old Quarry Road, Ridgefield, CT 06877.

(1) Fraissard, J.; Ito, T. *Zeolites* **1988**, *8*, 350−361.

(2) Barrie, P. J.; Klinowski, J. *Prog. Nucl. Magn. Reson. Spectrosc.* **1992**, *24*, 91−108.

(3) Jokisaari, J. *Prog. Nucl. Magn. Reson. Spectrosc.* **1994**, *26*, 1−25.

(4) Raftery, D.; Chmelka, B. F. In *NMR Basic Principles and Progress*; Blümich, B., Ed.; Springer-Verlag: Berlin, Heidelberg, 1994; Vol. 30; pp 111−158.

(5) Pietra*β*, T.; Gaede, H. *Adv. Mater.* **1995**, *7*, 826−838.

(6) Albert, M. S.; Balamore, D. *Nucl. Instrum. Meth. Phys. Res., Sect. A* **1998**, *402*, 441−453.

(7) Bartik, K.; Luhmer, M.; Heyes, S. J.; Ottinger, R.; Reisse, J. *J. Magn. Reson. B* **1995**, *109*, 164−168.

(8) Xu, Y.; Tang, P. *Biochim. Biophys. Acta* **1997**, *1323*, 154−162.

(9) Kastler, A. *J. Phys. Radium* **1950**, *11*, 255−265.

(10) Bouchiat, M. A.; Carver, T. R.; Varnum, C. M. *Phys. Rev. Lett.* **1960**, *5*, 373−375.

(11) Happer, W.; Miron, E.; Schaefer, S.; Schreiber, D.; van Wijngaarden, W. A.; Zeng, X. *Phys. Rev.* **1984**, *A29*, 3092−3110.

(12) Walker, T. G.; Happer, W. *Rev. Mod. Phys.* **1997**, *69*, 629−642.

(13) Cates, G. D.; Benton, D. R.; Gatze, M.; Happer, W.; Hasson, K. C.; Newbury, N. R. *Phys. Rev. Lett.* **1990**, *65*, 1591−2594.

(14) Raftery, D.; Long, H.; Meersmann, T.; Grandinetti, P. J.; Reven, L.; Pines, A. *Phys. Rev. Lett.* **1991**, *66*, 584−587.

(15) Gatzke, M.; Cates, G. D.; Driehuys, B.; Fox, D.; Happer, W.; Saam, B. *Phys. Rev. Lett.* **1993**, *70*, 690−693.

(16) Albert, M. S.; Cates, G. D.; Driehuys, B.; Happer, W.; Saam, B.; Springer, C. S., Jr.; Wishnia, A. *Nature* **1994**, *370*, 199−201.

(17) Song, Y.-Q.; Gaede, H. C.; Pietra*β*, T.; Barrall, G. A.; Chingas, G. C.; Ayers, M. R.; Pines, A. *J. Magn. Reson. A* **1995**, *115*, 127−130.

(18) Bifone, A.; Song, Y.-Q.; Seydoux, R.; Taylor, R. E.; Goodson, B. M.; Pietra*β*, T.; Budinger, T. F.; Navon, G.; Pines, A. *Proc. Natl. Acad. Sci. U.S.A.* **1996**, *93*, 12932−12936.

(19) Sauer, K. L.; Fitzgerald, R. J.; Happer, W. *Chem. Phys. Lett.* **1997**, *277*, 153−158.

(20) Mugler, J. P., III; Driehuys, B.; Brookeman, J. R.; Cates, G. D.; Berr, S. S.; Bryant, R. G.; Daniel, T. M.; de Lange, E. E.; Downs, J. H., III; Erikson, C. J.; Happer, W.; Hinton, D. P.; Kassel, N. F.; Maier, T.; Phillips, D.; Saam, B. T.; Sauer, K. L.; Wagshul, M. E. *Magn. Reson. Med.* **1997**, *37*, 809−815.

(21) Swanson, S. D.; Rosen, M. S.; Agranoff, B. W.; Coulter, K. P.; Welsh, R. C.; Chupp, T. E. *Magn. Reson. Med.* **1997**, *38*, 695−698.

(22) Augustine, M. P.; Wong-Foy, A.; Yarger, J. L.; Tomaselli, M.; Pines, A.; TonThat, D. M.; Clarke, J. *Appl. Phys. Lett.* **1998**, *72*, 1908−1910.

(23) Tseng, C. H.; Wong, G. P.; Pomeroy, V. R.; Mair, R. W.; Hinton, D. P.; Hoffmann, D.; Stoner, R. E.; Hersman, F. W.; Cory, D. G.; Walsworth, R. L. *Phys. Rev. Lett.* **1998**, *81*, 3785−3788.

(24) Jänsch, H. J.; Hof, T.; Ruth, U.; Schmidt, J.; Stahl, D.; Fick, D. *Chem. Phys. Lett.* **1998**, *296*, 146−150.

(25) Navon, G.; Song, Y.-Q.; Rõõm, T.; Appelt, S.; Taylor, R. E.; Pines, A. *Science* **1996**, *271*, 1848−1851.

10.1021/ja9841916 CCC: $18.00
Published on Web 03/30/1999

example, the xenon polarization can be transferred via cross-relaxation to molecules in solution[25−27] and to surfaces,[28−33] a process called the "spin polarization-induced nuclear Overhauser effect" (SPINOE). Temporary binding of xenon to the hydrophobic pocket of α-cyclodextrin was shown to yield distance-selective cross-relaxation rates, thereby enhancing the NMR signal of protons to a degree dictated by their proximity to the xenon binding site.[26] These results suggest that SPINOE polarization transfer could be utilized to study structure and dynamics in molecules that interact with xenon and to map their hydrophobic potentials. SPINOE experiments could also be used to identify those regions of macromolecules and biological systems that are accessible to and interact with xenon atoms.

Xenon is known to interact with a variety of systems,[7,8,34−48] including proteins in solution[34−36] and in crystals.[37−42] Recent work in proteins has been motivated by the desire to map hydrophobic sites and also to use xenon/protein complexes as heavy-atom derivatives for X-ray structure determination.[40−42] Studies using xenon dissolved in lipid vesicles as a model for anesthetic action showed that xenon is preferentially attracted to amphiphilic regions in lipid membranes.[8] Finally, xenon has been shown to form a variety of inclusion compounds with α-cyclodextrin,[7,43] hemicarcerands,[44,45] self-assembling dimers,[46] calixarenes,[47] and, most recently, cryptophane-A.[48]

Cryptophane-A (MW = 895.02 g/mol) is a nearly spherical cage molecule composed of two cyclotriveratrylene bowls connected by three OCH_2CH_2O spacer bridges (Figure 1). In a recent study, it was shown that the complex of xenon and

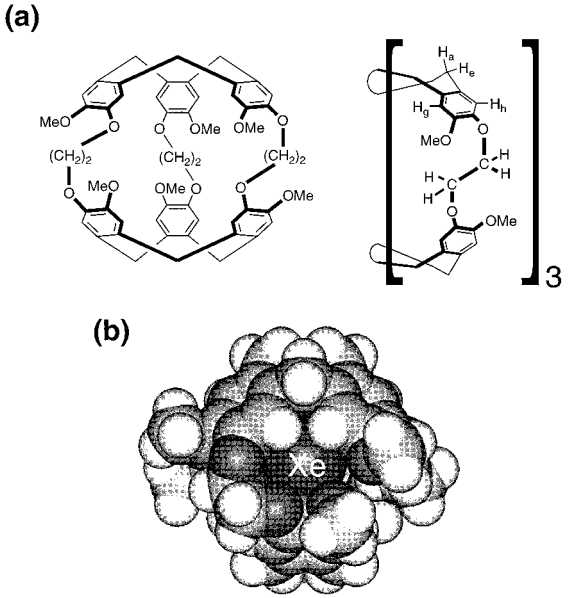

Figure 1. (a) Structure of cryptophane-A and atom labeling used in the ^{1}H spectrum (the assignment of the ^{1}H signals of the spacer bridges is discussed later). (b) CPK model of one possible conformation of cryptophane-A with a xenon atom placed within the binding pocket.

cryptophane-A in 1,1,2,2-tetrachloroethane exhibits particularly strong binding, with a reported association constant (K) greater than 3000 M^{-1} at 278 K,[48] whereas K for the xenon/α-cyclodextrin complex in H_2O has been reported to be on the order of 20 M^{-1}.[7,49] Unlike the complexes of xenon and hemicarcerands (which exhibit K's on the order of ∼200 M^{-1}),[44] the Xe/cryptophane-A complex is formed without a high degree of constrictive binding (i.e., trapped xenon is not required to overcome large steric constraints of the portals of cryptophane-A in order to escape confinement), giving xenon residence times on the order of milliseconds instead of hours.[48] The cryptophane-A molecule can adopt various conformations that affect the size of the cavity and the stability of the host−guest complex; the dynamics of the host are expected to influence the manner in which the guest is bound and released.[50]

In this paper we provide a general theoretical framework describing the SPINOE in solution, with stress placed on the interpretation of SPINOE results in terms of the interactions between xenon and its environment. We report ^{129}Xe NMR and SPINOE experiments for laser-polarized xenon interacting with cryptophane-A in solution. By using laser-polarized xenon, selective enhancements of the NMR signals of protons adjacent to the xenon binding site were observed, permitting experimentally derived ^{1}H−^{129}Xe cross-relaxation rates to be correlated with internuclear distances. Finally, by comparing experimen-

(26) Song, Y.-Q.; Goodson, B. M.; Taylor, R. E.; Laws, D. D.; Navon, G.; Pines, A. *Angew. Chem., Int. Ed. Engl.* **1997**, *36*, 2368−2370.
(27) Fitzgerald, R. J.; Sauer, K. L.; Happer, W. *Chem. Phys. Lett.* **1998**, *284*, 87−92.
(28) Rõõm, T.; Appelt, S.; Seydoux, R.; Pines, A.; Hahn, E. L. *Phys. Rev. B* **1997**, *55*, 11604−11610.
(29) Raftery, D.; MacNamara, E.; Fisher, G.; Rice, C. V.; Smith, J. *J. Am. Chem. Soc.* **1997**, *119*, 8746−8747.
(30) Haake, M.; Pines, A.; Reimer, J. A.; Seydoux, R. *J. Am. Chem. Soc.* **1997**, *119*, 11711−11712.
(31) Brunner, E.; Seydoux, R.; Haake, M.; Pines, A.; Reimer, J. A. *J. Magn. Reson.* **1998**, *130*, 145−148.
(32) Pietra*β*, T.; Seydoux, R.; Pines, A. *J. Magn. Reson.* **1998**, *133*, 299−303.
(33) Brunner, E.; Haake, M.; Pines, A.; Reimer, J. A.; Seydoux, R. *Chem. Phys. Lett.* **1998**, *290*, 112−116.
(34) Miller, K. W.; Reo, N. V.; Schoot Uiterkamp, A. J. M.; Stengle, D. P.; Stengle, T. R.; Williamson, K. L. *Proc. Natl. Acad. Sci. U.S.A.* **1981**, *78*, 4946−4949.
(35) Tilton, R. F., Jr.; Kuntz, I. D., Jr. *Biochemistry* **1982**, *21*, 6850−6857.
(36) McKim, S.; Hinton, J. F. *Biochim. Biophys. Acta* **1994**, *1193*, 186−198.
(37) Shoenborn, B. P.; Watson, H. C.; Kendrew, J. C. *Nature* **1965**, *207*, 28−30.
(38) Shoenborn, B. P. *Nature* **1965**, *208*, 760−762.
(39) Tilton, R. F., Jr.; Kuntz, I. D., Jr.; Pestko, G. A. *Biochemistry* **1984**, *23*, 2849−2857.
(40) Shlitz, M.; Prangé, T.; Fourme, R. *J. Appl. Crystallogr.* **1994**, *27*, 950−960.
(41) Shlitz, M.; Fourme, R.; Broutin, I.; Prangé, T. *Structure* **1995**, *3*, 309−316.
(42) Prangé, T.; Shlitz, M.; Pernot, L.; Colloc'h, N.; Longhi, S.; Bourget, W.; Fourme, R. *Proteins: Struct., Funct., Genet.* **1998**, *30*, 61−73.
(43) Ripmeester, J. A.; Ratcliffe, C. I.; Tse, J. S. *J. Chem. Soc., Faraday Trans. 1* **1988**, *84*, 3731−3745.
(44) Cram, D. J.; Tanner, M. E.; Knobler, C. B. *J. Am. Chem. Soc.* **1991**, *113*, 7717−7727.
(45) Robbins, T. A.; Knobler, C. B.; Bellew, D. R.; Cram, D. J. *J. Am. Chem. Soc.* **1994**, *116*, 111−122.
(46) Branda, N.; Grotzfeld, R. M.; Valdés, C.; Rebek, J., Jr. *J. Am. Chem. Soc.* **1995**, *117*, 85−88.
(47) Brouwer, E. B.; Enright, J.; Ripmeester, J. A. *Chem. Commun.* **1997**, 939−940.
(48) Bartik, K.; Luhmer, M.; Dutasta, J.-P.; Collet, A.; Reisse, J. *J. Am. Chem. Soc.* **1998**, *120*, 784−791.
(49) Hitchens, T. K.; Bryant, R. G. *J. Magn. Reson.* **1997**, *124*, 227.
(50) Kirchhoff, P. D.; Bass, M. B.; Hanks, B. A.; Briggs, J. M.; Collet, A.; McCammon, J. A. *J. Am. Chem. Soc.* **1996**, *118*, 3237−3246.
(51) Solomon, I. *Phys. Rev.* **1955**, *99*, 559−565.
(52) Noggle, J. H.; Schirmer, R. E. *The Nuclear Overhauser Effect: Chemical Applications*; Academic Press: New York, London, 1971.
(53) Cavanagh, J.; Fairbrother, W. J.; Palmer, A. G.; Skelton, N. J. *Protein NMR Spectroscopy: Principles and Practice*; Academic Press: San Diego, 1996.
(54) Song, Y.-Q., manuscript submitted for publication.
(55) Spin−lattice relaxation times of hundreds of seconds are usually observed for ^{129}Xe dissolved in most simple solvents. Binding of xenon to molecules such as α-cyclodextrin or cryptophane-A may shorten the relaxation time to tens of seconds, but this remains much longer than typical ^{1}H relaxation times. However, the interaction of xenon with paramagnetic molecules may considerably accelerate the relaxation; ^{129}Xe spin−lattice relaxation times on the order of 0.1 s have been observed in aqueous solutions of metmyoglobin (M. Luhmer, to be published).

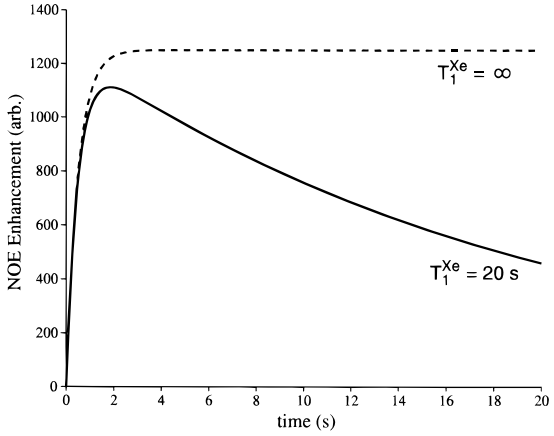

Figure 2. Calculated time dependence of the SPINOE signal, including (solid line) and not including (dotted line) the exponential decay caused by the eventual ^{129}Xe spin−lattice relaxation. Curves were calculated with $\rho_I = 2\ s^{-1}$, $\sigma_{IS} = 0.001\ s^{-1}$, and $\rho_S = 0.05\ s^{-1}$ (for the solid curve). Behavior such as that shown with the dotted line may also be seen under conditions of continuous flow of polarized xenon.[30]

tally obtained cross-relaxation rates with computational models, the preferred conformations of cryptophane-A in the xenon complex were determined.

II. Theoretical Background

II. 1. Solomon Equations for a Two-Spin System. Cross-relaxation between any two spins, *I* and *S*, is described by the Solomon equations[51,52]

$$\frac{dI_z}{dt} = -\rho_I(I_z - I_o) - \sigma_{IS}(S_z - S_o) \quad (1a)$$

$$\frac{dS_z}{dt} = -\rho_S(S_z - S_o) - \sigma_{SI}(I_z - I_o) \quad (1b)$$

where I_z and S_z are the average values of the *z* component of the **I** and **S** nuclear spin operators, and I_o and S_o are the equilibrium values ($I_o = I(I+1)\hbar\gamma_I B_o/3k_BT$ and similarly for spin *S*). The values ρ_I, ρ_S and σ_{IS}, σ_{SI} are respectively the auto-relaxation and cross-relaxation rate constants. A full solution to the Solomon equations can be found in the literature[53] and is discussed in a forthcoming review concerning the SPINOE.[54] If the nuclear spin−lattice relaxation of spin *S* is much slower than that of spin *I* (normally the case for $S = {}^{129}$Xe when dissolved in solution),[55] the change in the polarization of spin *I* is well-approximated by

$$f_I(t) = f_I(0)e^{-\rho_I t} - \frac{S_o}{I_o} f_S(0) \frac{\sigma_{IS}}{\rho_I}(1 - e^{-\rho_I t}) \quad (2)$$

where $f_I(t) = (I_z(t) - I_o)/I_o$ is the fractional polarization enhancement of spin *I* (and similarly for spin *S*). Equation 2 is the solution to eq 1a given a constant polarization of spin *S* and is valid in the short time limit (i.e., for times short relative to the spin−lattice relaxation time of spin *S*, $T_1^S = 1/\rho_S$) or when the *S* spin polarization is maintained by continuous flow (Figure 2).[30] The second term on the right side of eq 2 describes the time evolution of the polarization of spin *I* originating from $S \rightarrow I$ polarization transfer. For intermolecular polarization transfer, the magnitude of this term is often small with respect to the equilibrium polarization of spin *I* (except when laser-polarized xenon is used as a solvent[19,27,56]), requiring an NMR pulse sequence dedicated to the direct measurement of the SPINOE difference. Such a heteronuclear difference NOE pulse sequence is described in the Materials and Methods, in addition to a full version expression analogous to eq 2 that accounts for experimental considerations and the relaxation of spin *S*. Hereafter, an NMR spectrum obtained using this sequence will be referred to as a SPINOE spectrum.

II. 2. General Considerations for ^{129}Xe → ^{1}H Polarization Transfer. In the framework of the dipolar-coupled two-spin model, the auto-relaxation of spin *I* (^{1}H) is solely a consequence of dipole−dipole interactions with spin *S* (^{129}Xe). However, molecules in solution contain many spin systems; therefore, intermolecular ^{1}H−^{129}Xe dipole−dipole interactions are not likely to contribute significantly to the ^{1}H auto-relaxation rate. For solutes at low concentration in deuterated solvents, when no paramagnetic species are present, intramolecular ^{1}H−^{1}H dipole−dipole interactions are expected to dominate the auto-relaxation of protons in molecules large enough to bind xenon (although other mechanisms, such as spin−rotation coupling, may contribute to the relaxation of small molecules such as benzene or parts of molecules, like methyl groups). Therefore, the simplest realistic model for ^{129}Xe → ^{1}H polarization transfer requires at least a three-spin system: two interacting ^{1}H's and one ^{129}Xe in dipolar interaction with one of the ^{1}H sites. A three-spin model is presented in the Appendix and will be used in the discussion of the dynamics of ^{129}Xe → ^{1}H polarization transfer. However, for the purpose of interpreting experimental SPINOE spectra, the two-spin model is sufficient, remembering that in eq 2, $\rho_I \approx 1/T_1^H$, where T_1^H is the experimental spin−lattice ^{1}H relaxation time (see eq 3). Finally, because both ^{1}H and ^{129}Xe nuclei have a spin quantum number of $^1/_2$, the ratio S_o/I_o is equal to the ratio of the gyromagnetic ratios, γ_{Xe}/γ_H (and is negative, due to the negative value of γ_{Xe}). Equation 2 can then be rewritten as

$$f_H(t) = f_H(0)\, e^{-t/T_1^H} - \frac{\gamma_{Xe}}{\gamma_H} f_{Xe}(0)\, \sigma_{HXe}\, T_1^H (1 - e^{-t/T_1^H}) \quad (3)$$

By using the measured ^{1}H enhancements, and provided that the ^{1}H relaxation times and the ^{129}Xe polarization are known, eq 3 may be used to obtain the H−Xe cross-relaxation rates, σ_{HXe}.

II. 3. General Considerations for ^{1}H−^{129}Xe Cross-Relaxation Rates. The quantity σ_{HXe} largely controls the ^{129}Xe → ^{1}H polarization transfer. Assuming an exponential decay for the H−Xe dipole−dipole interaction correlation function, the cross-relaxation rate is given by[52]

$$\sigma_{HXe} = \left(\frac{\mu_o}{4\pi}\right)^2 \frac{\hbar^2\gamma_H^2\gamma_{Xe}^2}{10}\left\langle\frac{1}{r_{HXe}^6}\right\rangle[6J(\omega_H + \omega_{Xe}) - J(\omega_H - \omega_{Xe})] \quad (4a)$$

$$\text{with} \quad J(\omega) = \frac{\tau_c}{1 + \omega^2\tau_c^2} \quad (4b)$$

where τ_c is the correlation time associated with the fluctuations of the H−Xe dipole−dipole interactions, r_{HXe} is the H−Xe internuclear distance, and $\langle\ \rangle$ denotes the ensemble average.

Both $\langle r_{HXe}^{-6}\rangle$ and τ_c control the amplitude and selectivity of the ^{129}Xe → ^{1}H polarization transfer. The dependence of σ_{HXe}

(56) (a) Haake, M.; Seydoux, R.; Reimer, J. A.; Pines, A. In *39th Rocky Mountain Conference on Analytical Chemistry*; Denver, CO, 1997. (b) Haake, M.; Goodson, B. M.; Laws, D. D.; Brunner, E.; Cyrier, M. C.; Havlin, R. H.; Pines, A. *Chem. Phys. Lett.* **1998**, *292*, 686−690. (c) Tseng, C. H.; Mair, R. W.; Wong, G.; Williamson, D.; Cory, D. G.; Walsworth, R. L. *Phys. Rev. E: Stat. Phys., Plasmas, Fluids, Relat. Interdiscip. Top.*, in press.

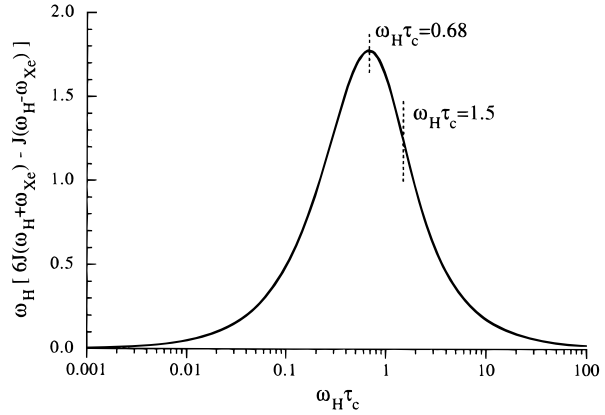

Figure 3. Illustration of the dependence of the $^1H-^{129}Xe$ cross-relaxation rate, σ_{HXe}, on the correlation time, where $\omega_H[6J(\omega_H + \omega_{Xe}) - J(\omega_H - \omega_{Xe})] = 6\omega_H\tau_c/[1 + (1 + |\gamma_{Xe}/\gamma_H|)^2\omega_H^2\tau_c^2] - \omega_H\tau_c/[1 + (1 - |\gamma_{Xe}/\gamma_H|)^2\omega_H^2\tau_c^2]$.

on the correlation time can be understood from Figure 3 where $\omega_H[6J(\omega_H + \omega_{Xe}) - J(\omega_H - \omega_{Xe})]$ is displayed as a function of $\omega_H\tau_c$. The function indicates that σ_{HXe} is always positive and has its maximum value at $\omega_H\tau_c \approx 0.68$. An increase in the correlation time from a few ps ($\omega_H\tau_c = 0.01-0.02$) to a value corresponding to the maximum (τ_c in the range 0.2−0.5 ns) gives rise to a ~20-fold increase in σ_{HXe}. However, this increase does not necessarily translate into an increase in the observed SPINOE enhancement. Indeed, in real systems large enough to bind xenon, the increased correlation time characterizing the H−Xe dipole−dipole interactions would generally be accompanied by a corresponding increase in the correlation time characterizing the H−H dipole−dipole interactions, and a concomitant reduction of T_1^H (see eq 3). A more thorough discussion of this argument may be found in the Appendix.

II. 4. $^1H-^{129}Xe$ Cross-Relaxation Rates and Solute−Xenon Intermolecular Interactions. The value of σ_{HXe} depends on H−Xe dipole−dipole interactions which change with the structural and dynamical characteristics of the intermolecular couplings between xenon and its molecular environment. A given molecule, M, may participate in various types of interactions with a xenon atom including nonspecific interactions (i.e., diffusive coupling), preferential solvation, and xenon binding (the formation of a Xe:M complex). Exchange phenomena are involved between these various situations, but the exchange is generally rapid with respect to both the ^1H and ^{129}Xe relaxation rates. Furthermore, ^1H chemical shifts are expected to be poorly sensitive to intermolecular interactions with xenon, and therefore fast-exchange conditions with respect to the ^1H chemical shift NMR time scale are also likely to be fulfilled. This behavior implies that the ^1H spectrum will not be resolved according to the solute−xenon interactions and that the observed ^1H SPINOE enhancement may originate from a combination of interaction modes. Therefore, the experimental H−Xe cross-relaxation rate is most generally written as

$$\sigma_{HXe} = \sum_i \frac{[M]_i}{[M]_T}\sigma^i_{HXe} \qquad (5)$$

where the summation runs over the interaction modes, $[M]_T$ is the total concentration of the solute, $[M]_i$ is the molar concentration of the solute involved in the interaction mode *i*, and σ^i_{HXe} is the H−Xe cross-relaxation rate associated with that mode.

For a dilute solution of xenon-binding molecules, a simple model considers two modes of interaction: diffusive coupling, σ^d_{HXe}, which exists for any kind of solute molecule, and xenon binding, σ^b_{HXe}, which gives rise to the formation of a 1-to-1 xenon:host complex

$$\sigma_{HXe} = \sigma^d_{HXe} + \frac{[Xe:M]}{[M]_T}\sigma^b_{HXe} \qquad (6)$$

In eq 6, it is assumed that both "empty" host molecules and molecules with included xenon (hereafter, included xenon is referred to as Xe_{in}) experience identical diffusive coupling with unbound xenon (referred to as Xe_{out}); [Xe:M] is the equilibrium molar concentration of the xenon:host complex ([Xe:M] ≡ $[Xe]_{in}$).

II. 4a. The $^1H-^{129}Xe$ Cross-Relaxation Rate Due to Diffusive Coupling. A proper description of the intermolecular cross-relaxation originating from diffusive coupling requires a detailed microscopic understanding of the structure and dynamics of solutions. Although molecular dynamics simulations are very helpful for characterizing intermolecular relaxation,[57,58] they tend to be computationally demanding. However, simpler models of intermolecular relaxation can be found in the literature[52] that rely on crude assumptions yet provide reasonable qualitative descriptions of the intermolecular dipole−dipole relaxation process. For example, it can be shown that σ_{IS} should be linearly dependent on the concentration of molecules bearing spin *S*; thus, σ^d_{HXe} is dependent on $[Xe]_{out}$. Such a dependence, in fact, arises from the ensemble average of r^{-6}_{HXe}. In a pairwise additivity scheme for xenon-solute interactions, $\langle r^{-6}_{HXe}\rangle^d$ is given by

$$\langle r^{-6}_{HXe}\rangle^d = \left[4\pi N_A 10^{-27}\int_0^\infty dR\, R^2\, \frac{\int d\Omega\, g(R,\Omega)\, r^{-6}_{HXe}}{\int d\Omega}\right][Xe]_{out} \qquad (7)$$

where *R* is the distance between the center-of-mass of the solute molecule and the xenon atom (with *R* and r_{HXe} in Å), N_A is Avogadro's number, Ω represents the angular variables specifying the relative orientation of the solute−xenon pair, and $g(R, \Omega)$ is the solute−xenon pair distribution function. To a good approximation, $\langle r^{-6}_{HXe}\rangle^d$ is proportional to $[Xe]_{out}$; and therefore, a concentration-normalized H−Xe cross-relaxation rate, σ^n_{HXe} ($s^{-1}\cdot M^{-1}$), may be defined according to the relation

$$\sigma^d_{HXe} = \sigma^n_{HXe}\,[Xe]_{out} \qquad (8)$$

Concerning the dynamics of the diffusive coupling, it is clear that an upper bound for the correlation time τ^d_c is provided by the residence time of xenon in the solvation shell of the solute. In common solvents, τ^d_c is in the range of 10^{-12} to 10^{-11} s, and the condition of extreme narrowing is thereby fulfilled.[59] The

(57) Luhmer, M.; Moschos, A.; Reisse, J. *J. Magn. Reson. A* **1995**, *113*, 164−168.

(58) Luhmer, M.; Reisse, J. *Prog. Nucl. Magn. Res. Spectrosc.* **1998**, *33*, 57−76.

(59) Using molecular dynamics simulations, the correlation time associated with the fluctuations of the intermolecular H−Xe dipole−dipole interactions has been estimated to be ~5 ps for xenon dissolved in benzene. It was found that this correlation time depends on both the rotational motions of the benzene molecules and the translation of xenon relative to benzene. However, the translational motions were found to be the most important contribution.[58]

(60) Xenon−solute pair configurations with lifetimes significantly longer than the average residence time of xenon in the solute solvation shell, but short-lived in the sense that they do not reorient as a whole, could be regarded as specific preferential solvation.

^{1}H−^{129}Xe cross-relaxation rate due to diffusive coupling is then given by

$$\sigma^{d}_{HXe} = \left(\frac{\mu_o}{4\pi}\right)^2 \frac{\hbar^2 \gamma_H^2 \gamma_{Xe}^2}{10} \langle r_{HXe}^{-6} \rangle^d \, 5\tau_c^d \qquad (9)$$

It is worth noting that τ_c^d may be unrelated to the correlation time controlling the ^{1}H dipole−dipole intramolecular relaxation of the solute molecule. For instance, in circumstances where the molecular mass of the solute significantly exceeds the xenon atomic mass, the tumbling motion of the solute molecules is expected to be slow on the time scale of the residence of xenon atoms in the solvation shell of the solute. As a consequence, the importance of the SPINOE signal originating from diffusive coupling is expected to decrease for increasing solute size, not because σ^d_{HXe} is affected, but because T_1^H is reduced (see eq 3 and the Appendix for more details).

The order of magnitude of σ^n_{HXe} and σ^d_{HXe} can now be estimated by assuming the system is a monatomic fluid and by using a Heaviside step function as an approximation for the radial pair distribution function [$g(r) = 0$ for $r < r_o$ and 1 otherwise] in eq 7, leading to $\langle r_{HXe}^{-6} \rangle^d \approx 4\pi N_A 10^{-27}$ $^1/_3 r_o^{-3} \cdot [Xe]_{out}$, where r_o is the proton−xenon minimum approach distance. Using this result and eqs 8 and 9, with $\tau_c^d = 5$ ps and r_o in the range 3.0−3.2 Å, σ^n_{HXe} is estimated to be on the order of 10^{-5} $s^{-1} \cdot M^{-1}$, a figure in agreement with experimental results.[25,26] Because the solubility of xenon in organic solvents under standard conditions is on the order of 0.1 M, σ^d_{HXe} is expected to be on the order of 10^{-6} s^{-1}.

II. 4b. The ^{1}H−^{129}Xe Cross-Relaxation Rate Due to Binding. Binding of xenon implies that a particular configuration of a xenon−solute pair has a lifetime long enough that it can be considered as a supramolecule. The time scale relevant to ^{129}Xe → ^{1}H polarization transfer is the correlation time, τ_r, for the tumbling motion of the transient Xe−solute pair; binding implies that the lifetime of the Xe−solute pair is much longer than the correlation time for its overall tumbling motion,[60] and therefore, the latter controls the dynamics of σ^b_{HXe}. Under these circumstances, the description of the Xe−H cross-relaxation rate reduces to the intramolecular case, and eq 4 may be used with $\tau_c^b = \tau_r$ to obtain H−Xe average distances that characterize the structure of the xenon-host complex. Naturally, the validity of such an analysis of experimental σ^b_{HXe} data depends on the importance of internal dynamics. The consequences of internal motions of the host molecule, in addition to the motion of xenon inside the binding site, are $\tau_c^b < \tau_r$ and $\langle r_{HXe}^{-6} \rangle^b$ values which may be difficult to interpret because they correspond to weighted averages over multiple configurations. In such cases, molecular dynamics simulations may be helpful.

An upper bound for σ^b_{HXe} can be estimated from eq 4 using $\omega_H \tau_c^b = 0.68$ (from Figure 3) and $\langle r_{HXe}^{-6} \rangle^b = (3.2 \text{ Å})^{-6}$ (an estimate of the minimum approach distance of Xe and H). For a ^{1}H resonance frequency of 400 MHz, these numbers correspond to a σ^b_{HXe} value of 3×10^{-3} s^{-1}, a figure which is 3 orders of magnitude larger than the value expected for the ^{1}H−^{129}Xe cross-relaxation rate due to diffusive coupling. Indeed, σ^b_{HXe} values of this order have been observed for xenon bound to α-cyclodextrin in solution.[26]

II. 4c. Xenon Concentration Dependence of the Experimental ^{1}H−^{129}Xe Cross-Relaxation Rate. In Section II. 4a, it was shown that σ^d_{HXe} is, to a good approximation, proportional to the concentration of unbound xenon. An additional concentration dependence of the experimental cross-relaxation rate may arise from the effect of the xenon concentration on the binding equilibrium. On the basis of the definition of the binding constant, K, for the equilibrium $Xe_{out} + M \rightleftharpoons Xe{:}M$, the following relationships hold

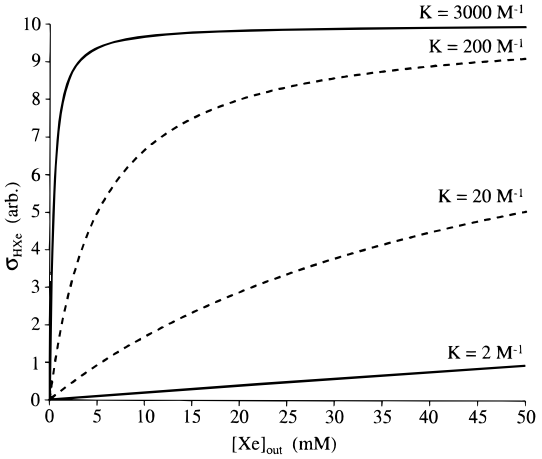

Figure 4. Dependence of experimental Xe−H cross-relaxation rate (σ_{HXe}) originating from xenon binding on the equilibrium xenon concentration in the solvent for various association constants, K. Curves with solid lines are for systems that have been studied via SPINOE experiments (Xe/cyclodextrin in DMSO, $K = 2$ M^{-1}; Xe/cryptophane-A in $(CDCl_2)_2$, $K = 3000$ M^{-1}). The dotted curves, added for illustrative purposes, correspond to what would be expected for Xe/cyclodextrin in H_2O, $K \approx 20$ M^{-1},[7,49] and xenon/myoglobin or xenon/hemicarcerand, $K \approx 200$ M^{-1}.[35,44]

$$\frac{[Xe{:}M]}{[M]_T} = \frac{K[Xe]_{out}}{1 + K[Xe]_{out}} \qquad (10a)$$

which for the case of weak binding reduces to:

$$\frac{[Xe{:}M]}{[M]_T} \approx K[Xe]_{out} \qquad (10b)$$

and for the case of strong binding and excess xenon reduces to:

$$\frac{[Xe{:}M]}{[M]_T} \approx 1 \qquad (10c)$$

Equation 10 is written in terms of $[Xe]_{out}$, and not as a function of the total concentration in xenon, because for dilute solutions of host molecules, $[Xe]_{out}$ is well-approximated by the equilibrium solubility of xenon in the pure solvent. For example, an equilibrium constant of ∼2 M^{-1} has been reported for the binding of xenon to cyclodextrin in DMSO (298 K).[7] For an equilibrium xenon pressure of 1 atm, the solubility of xenon in DMSO is 0.024 M (298 K). Therefore, eq 10b applies to this system, and a linear increase in the SPINOE originating from binding is expected upon increasing xenon pressures (at least for pressure in the range of 0−3 atm), as shown in Figure 4. However, in tetrachloroethane (xenon solubility ∼0.1 M[61]), the equilibrium constant for the binding of xenon to cryptophane-A was estimated to be larger than 3000 M^{-1} (278 K);[48] therefore, eq 10c is more appropriate (Figure 4). Using eqs 8 and 10a, eq 6 can now be rewritten, taking into account the isotopic abundance in ^{129}Xe, A_{129}

$$\sigma_{HXe} = A_{129}\left[\sigma^n_{HXe}[Xe]_{out} + \frac{K[Xe]_{out}}{1 + K[Xe]_{out}}\sigma^b_{HXe}\right] \qquad (11)$$

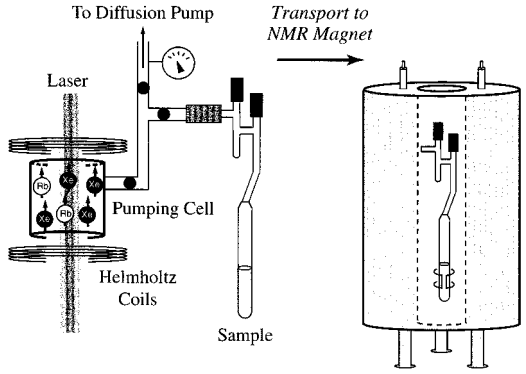

Figure 5. Experimental schematic. Continuous-wave circularly polarized light (1.3 W) tuned to the Rb D_1 transition (794.7 nm) originating from a Ti:sapphire laser is directed into a Pyrex pumping cell containing xenon gas and a small amount of Rb metal. The Xe is pumped in a weak, homogeneous magnetic field (~30 G) produced by a Helmholtz coil pair. The gas transfer line is evacuated to $\sim 10^{-5}$ Torr throughout the pumping process to prevent contamination from paramagnetic molecular oxygen. Following optical pumping, the xenon is cryopumped to the sidearm of the sample tube with liquid-N_2; the frozen xenon is kept at high field (~0.1 T) with a small permanent magnet to maintain the high nonequilibrium polarization. The sample is then transported to the NMR magnet, where the xenon is rapidly sublimated and delivered to the solution prior to signal acquisition.

III. Materials and Methods

Cryptophane-A, synthesized according to a procedure described elsewhere,[62,63] was provided by A. Collet and co-workers. Deuterated 1,1,2,2-tetrachloroethane, $(CDCl_2)_2$, was purchased from Aldrich and used without further purification. Approximately 2 mL of a ~0.05 M solution of cryptophane-A in $(CDCl_2)_2$ was placed in a 10-mm NMR tube equipped with a sidearm, and Teflon stopcocks were used to isolate the sample and the sidearm from each other and from the atmosphere. Helium gas was gently bubbled through the solution for 5−10 min to displace any other gases complexed by cryptophane-A. The sample was then degassed by several freeze−pump−thaw cycles on a vacuum line.

The optical pumping procedure is shown schematically in Figure 5;[13,14] the ^{129}Xe polarization was typically in the range 1−10%. Quantities of $(2-5) \times 10^{-4}$ mol of isotopically enriched xenon gas (80% ^{129}Xe, Isotec) were used in each experiment. Following optical pumping, laser-polarized ^{129}Xe was frozen into the sidearm of the NMR tube, transported to the spectrometer, and sublimated in the fringe field of the NMR magnet. After the xenon reservoir was opened, the sample tube shaken, and the tube inserted into the magnet, the NMR experiment was immediately performed. Generally, additional experiments could be performed by administering freshly polarized xenon to the solution by simply reshaking the sample tube.

^{1}H and ^{129}Xe NMR spectra were recorded at room temperature (~22 °C) on a Varian/Chemagnetics CMX-400 Infinity NMR spectrometer operating at a ^{1}H frequency of 400.15 MHz (nominal frequency for ^{129}Xe = 110.70 MHz). Laser-polarized ^{129}Xe NMR spectra were obtained using rf pulses of small tipping angle (typically 1−5°) to preserve ^{129}Xe magnetization. Measurements of ^{1}H T_1's were made using the inversion−recovery technique and determined using a 3-parameter nonlinear least-squares fitting procedure.

The SPINOE spectra were obtained using the NMR pulse sequence shown in Figure 6. This sequence is a variant of a difference NOE sequence developed by Shaka and co-workers[64,65] capable of efficiently

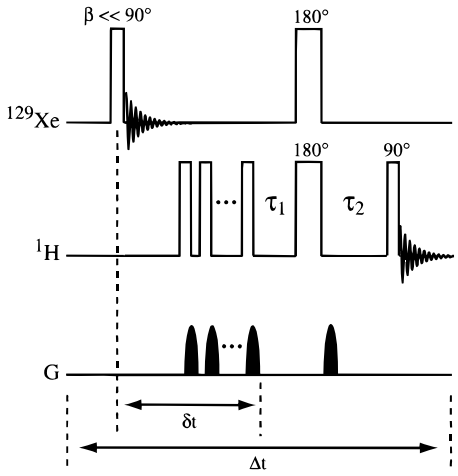

Figure 6. Heteronuclear difference NOE pulse sequence for ^{129}Xe−^{1}H SPINOE NMR experiments.

suppressing the equilibrium signal, thus permitting the direct observation of NOE signals as low as $\sim 1 \times 10^{-4}$ of the equilibrium signal. Prior to the detection of ^{1}H SPINOE signals, the polarization of ^{129}Xe is measured using a pulse of small tipping angle. The equilibrium ^{1}H signals are first saturated by 90° and gradient pulses, and the saturation is maintained by a 180° pulse followed immediately by a gradient pulse. A ^{129}Xe 180° pulse allows SPINOE signals to accumulate during the mixing periods τ_1 and τ_2. The total mixing period, $\tau = \tau_1 + \tau_2$, was in the range of the ^{1}H T_1's but was short compared to the ^{129}Xe T_1. The ratio τ_1/τ_2 is chosen to minimize the overall equilibrium ^{1}H signal observed in the absence of ^{1}H−^{129}Xe cross-relaxation. The 180° ^{1}H and ^{129}Xe inversion pulses are experimentally optimized BIR4 adiabatic inversion pulses.[66] Because the ^{129}Xe spectrum of the cryptophane-A solution consisted of two broad peaks separated by about 18 kHz, it was difficult to achieve perfect inversion. It is therefore necessary to explicitly account for the efficiency of the ^{129}Xe inversion pulses when calculating the experimental cross-relaxation rates (see below). Each ^{1}H SPINOE spectrum is the difference of two acquisitions. The resulting ^{1}H SPINOE signal is given by the following relation:

$$f_I^{(2)}(\tau) - f_I^{(1)}(\tau) = -\frac{S_o}{I_o}(f_S^{(1)} + f_S^{(2)})\cos(\beta)e^{-\rho_s \delta t}\frac{\sigma_{IS}}{\rho_I}\{(1 - e^{-\rho_I \tau}) - (1 - r)(1 - e^{-\rho_I \tau_2})\} \quad (12)$$

where the superscripts (1) and (2) denote the first and second acquisitions, and $f_S^{(1)} + f_S^{(2)}$ is the fractional ^{129}Xe enhancement determined from the observed ^{129}Xe signal (hereafter referred to as f_{Xe}^{obs}). Equation 12 is obtained from eq 2 under the following considerations: (i) The ^{129}Xe auto-relaxation has no effect on the polarization transfer (an approximation used in eq 2), but its overall effect on the xenon polarization must be considered; the factor $e^{-\rho_s \delta t}$ accounts for the decay of ^{129}Xe magnetization during the time interval between its measurement and the beginning of the SPINOE measurement (see Figure 6). (ii) While the ^{1}H 180° pulse is considered to produce complete inversion, the ^{129}Xe inversion was generally less efficient, and therefore the ^{129}Xe inversion efficiency, r, is explicitly included, where $0 < r < 1$ (experimentally determined r values varied from ~0.5−0.8). The term $(1 - r)(1 - e^{-\rho_I \tau_2})$ accounts for the smaller SPINOE during the delay τ_2 originating from the loss of ^{129}Xe polarization incurred from inefficient inversion. Additionally, these considerations imply the relationship $f_S^{(2)} = f_S^{(1)} \cos(\beta) r e^{-\rho_s \Delta t}$ (see Figure 6). Finally, by including the considerations of Section II. 2. eq 12 can be rewritten as

(61) The solubility of xenon in tetrachloroethane is not reported in the literature but is expected to be similar to the solubility in chloroform (0.14 M at 298 K and 1 atm).

(62) Canceill, J.; Collet, A. *J. Chem. Soc., Chem. Commun.* **1981**, 1137−1139.

(63) Canceill, J.; Collet, A. *J. Chem. Soc., Chem. Commun.* **1988**, 582−584.

(64) Stonehouse, J.; Adell, P.; Keeler, J.; Shaka, A. J. *J. Am. Chem. Soc.* **1994**, *116*, 6037−6038.

(65) Stott, K.; Keeler, J.; Van, Q. N.; Shaka, A. J. *J. Magn. Reson.* **1997**, *125*, 302−324.

(66) Garwood, M.; Ke, Y. *J. Magn. Reson.* **1991**, *94*, 511−525.

(67) Clifford, A. A.; Gray, P.; Platts, N. *J. Chem. Soc. Fraday. Trans. 1* **1977**, *73*, 381−382.

$$\Delta f_H(\tau) = -\frac{\gamma_{Xe}}{\gamma_H} f_{Xe}^{obs}(0)\cos(\beta)e^{-\delta t/T_1^{Xe}} \sigma_{HXe} T_1^H\{(1 - e^{-\tau/T_1^H}) - (1 - r)(1 - e^{-\tau_2/T_1^H})\} \quad (13)$$

Computer modeling of the Xe/cryptophane-A complex was carried out using the software Chem3D Plus from Cambridge Scientific Computing, Inc. The interaction parameters for xenon were user-defined, and correspond to a Xe−Xe Lennard−Jones interaction potential with $\sigma = 3.90$ Å and $\epsilon = 251.5$ K.[67]

IV. Results and Discussion

IV. 1. ^{129}Xe and ^{1}H Spin−Lattice Relaxation Times. Figure 7 shows ^{129}Xe NMR spectra of xenon dissolved in the cryptophane-A solution, with (Figure 7a) and without (Figure 7b) laser-polarization. The ^{129}Xe spectrum exhibits two lines separated by ∼160 ppm and considerably broadened due to chemical exchange. The higher field signal corresponds to the xenon trapped in the cryptophane-A cavity, Xe_{in}, with a chemical shift ∼60 ppm downfield with respect to the xenon gas resonance extrapolated to zero pressure. The trapping of xenon by cryptophane-A has been thoroughly studied by Reisse, Collet, and co-workwers.[48] The spectrum in Figure 7a was obtained with one scan using a rf pulse of small tipping angle (∼2.5°). In contrast, using thermally polarized ^{129}Xe, a comparable signal-to-noise ratio requires several hours of signal averaging.

As shown in Figure 8, the integrated intensities of both Xe_{in} and Xe_{out} decrease with the same time evolution, indicating that the relaxation of ^{129}Xe is a slow process compared to xenon exchange. The average T_1 of ^{129}Xe, T_1^{ave}, was found to be 22.1 s when the molar fraction of Xe_{in} was 0.74. The relaxation time of unbound ^{129}Xe is very long (hundreds of seconds in pure $(CDCl_2)_2$) and does not contribute significantly to the average relaxation time. On the basis of the molar fraction of Xe_{in}, the relaxation time of included ^{129}Xe, $T_1^{ave}\cdot[Xe_{in}/(Xe_{in} + Xe_{out})]$, was estimated to be 16.4 s. From a second experiment with a Xe_{in} molar fraction of 0.92, the relaxation time of trapped ^{129}Xe was estimated to be 16.2 s. The ^{1}H T_1 values for cryptophane-A are listed in Table 1. The longest relaxation times, ∼0.8 s, are those of the methoxy and aromatic hydrogens. Thus relaxation of ^{129}Xe in this system is slow with respect to ^{1}H relaxation and eq 2 (or eq 13) can be used when considering ^{129}Xe → ^{1}H SPINOE polarization transfer.

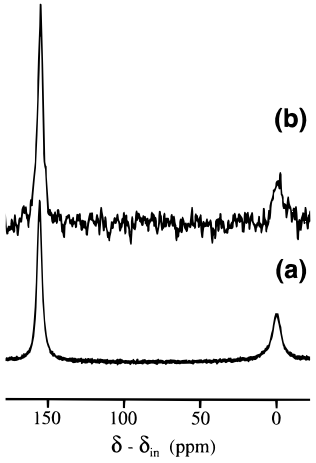

Figure 7. Typical ^{129}Xe NMR spectra for xenon dissolved in cryptophane-A/$(CDCl_2)_2$ solution, with (a) and without (b) laser-polarization. Spectrum (a) was acquired with one scan using a pulse of small tipping angle (∼2.5°); spectrum (b) was acquired with 8 scans using 90° pulses with a delay of 60 s between acquisitions. The ^{129}Xe spectra are referenced to the signal corresponding to xenon bound to cryptophane-A (Xe_{in}). A second signal can be seen roughly 160 ppm downfield from that of Xe_{in}, corresponding to unbound xenon residing in the $(CDCl_2)_2$ solvent (Xe_{out}). ^{129}Xe was in considerable excess for these experiments, as reflected by $[Xe]_{in} < [Xe]_{out}$.

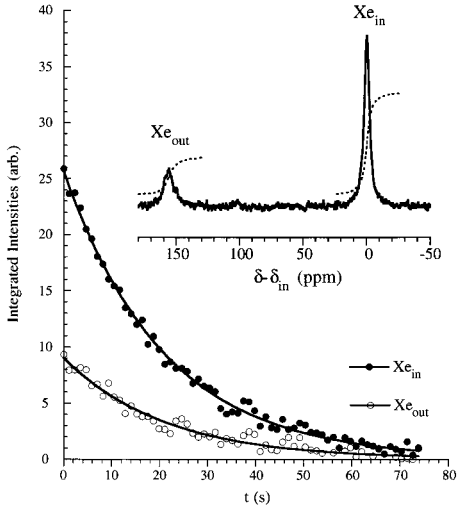

Figure 8. ^{129}Xe NMR spectrum of laser-polarized xenon dissolved in a ∼0.05 M solution of cryptophane-A in $(CDCl_2)_2$ and time evolution of the integrated intensities. The small amount of xenon used in this experiment is reflected in the fact that $[Xe]_{in} > [Xe]_{out}$.

Table 1. Spin−Lattice Relaxation Times, SPINOE Enhancements, Relative H−Xe Cross-Relaxation Rates, and Calculated Relative Values in Gauche Conformations for the Various Protons of Cryptophane-A[a]

proton	type	T_1^H (s)	SPINOE[a] (%)	$\sigma^b_{HXe}/\sigma^b_{H_{g,h}Xe}$	$\langle r^{-6}_{HXe}\rangle^b/\langle r^{-6}_{H_{g,h}Xe}\rangle^b$
aromatic	H_g, H_h	0.80	11.0	(1.00)	(1.00)
axial	H_a	0.27	3.0	0.47	0.3−0.4
linker	H_j, $H_{j'}$	0.36	5.2	0.67	0.3
linker	H_k, $H_{k'}$	0.41	13.0	1.55	1.5−1.8
methoxy	Me	0.83	2.6	0.23	0.1−0.3
equatorial	H_e	0.35	2.7	0.35	0.3−0.4

[a] SPINOE experiments were performed using the pulse sequence in Figure 6 with $\tau = 0.5$ s, $\tau_1/\tau_2 = 1.7$, and $\beta \approx 1°$. The following quantities were determined experimentally: the efficiency of the 180° pulse on ^{129}Xe was $r = 0.75$, the enhancement of the ^{129}Xe polarization $\approx 1.3 \times 10^4$ (error on the order of 50% is expected for this value), and the molar fraction of Xe_{in} was 0.33 (corresponding to $[Xe]_{out} \approx 0.1$ M). [b] Errors are estimated to be in the range 15−20%.

IV. 2. Tumbling Motion of Cryptophane-A. The rotational correlation time of cryptophane-A dissolved in $(CDCl_2)_2$ was determined on the basis of CW-driven ^{1}H−^{1}H NOE experiments. At room temperature, negative NOEs were observed. However, an increase in temperature of approximately 20 °C led to the observation of positive NOEs. This indicates that at room temperature, $\omega_H\tau_r$ has a somewhat higher value than 1.12, the point at which the ^{1}H−^{1}H cross-relaxation rate is equal to zero. The buildup of the NOE experienced by the equatorial protons, H_e, upon selective irradiation of the axial protons, H_a, was recorded at room temperature for saturation times ranging between 0.125 and 2.0 s (Figure 9). The steady-state NOE enhancement, η, and the auto-relaxation rate, ρ_{He} were measured to be −0.148 and 3.64 s^{-1}, respectively; these values correspond to a cross-relaxation rate $\sigma_{HeHa} = -0.54$ s^{-1}. Using eq A 4b with $r_{HeHa} = 1.72$ Å (determined from computer modeling of crytophane-A, see below), the correlation time was estimated to be 0.60 ns, and $\omega_H\tau_r = 1.5$ (nominal ^{1}H frequency: 400 MHz). Assuming that this correlation time controls the ^{129}Xe → ^{1}H polarization transfer originating from trapped xenon ($\tau_c^b = \tau_r$,

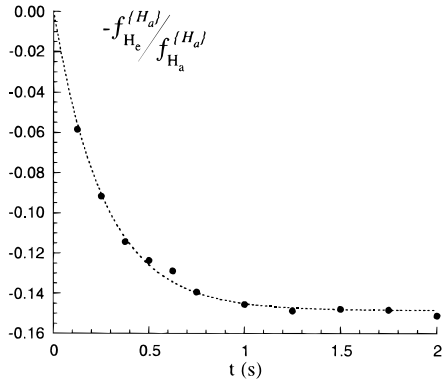

Figure 9. Time dependence of the NOE experienced by the equatorial protons (H_e) of cryptophane-A upon selective irradiation of the axial protons (H_a) at room temperature.

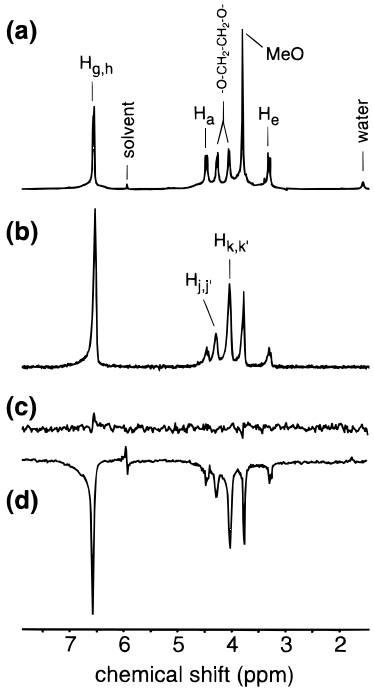

Figure 10. (a) ^{1}H NMR equilibrium spectrum of ~0.05 M cryptophane-A in $(CDCl_2)_2$ with chemical shift assignments. (b) ^{1}H SPINOE spectrum acquired with the pulse sequence shown in Figure 6 following the introduction of positively polarized ^{129}Xe to the solution. (c) As in (b), but with ^{129}Xe at thermal equilibrium, demonstrating virtually complete suppression of all contributions to the ^{1}H NMR signal. (d) ^{1}H SPINOE spectrum acquired during a second experiment in which negatively polarized ^{129}Xe (prepared by inverting the direction of the magnetic field in which the ^{129}Xe is laser-polarized) was used, resulting in a corresponding sign change in the ^{1}H SPINOE spectrum. Values of $\tau_1 = 315$ ms and $\tau_2 = 185$ ms were used for the SPINOE experiments shown.

see Section II. 4b), Figure 3 indicates that σ^b_{HXe}'s on the order of 70% of the maximum value can be expected.

IV. 3. SPINOE Spectra of Cryptophane-A and The Magnitude of ^{1}H−^{129}Xe Cross-Relaxation Rates. The equilibrium ^{1}H NMR spectrum of the cryptophane-A solution is shown in Figure 10a. The assignment of the cryptophane-A signals can be found elsewhere;[48] the proton NMR signals of the spacer bridges (which comprise an AA′BB′ spin system) are discussed below. Parts b−d of Figure 10 respectively show SPINOE spectra obtained with positively laser-polarized ^{129}Xe, with ^{129}Xe at equilibrium, and with negatively laser-polarized ^{129}Xe. The relative intensities in the SPINOE spectra (Figure 10b and d) differ from those in the equilibrium spectrum. The equilibrium spectrum is dominated by the signal of the methoxy group, while in the SPINOE spectra the signal from the aromatic protons is the most intense. The observed ^{1}H enhancements in Figure 10b range between 3 and 13% (see Table 1). Additionally, it is clear that the selectivity of the SPINOE is not primarily a consequence of unequal ^{1}H relaxation times, as the T_1^H's for the methoxy and aromatic protons are similar.

The determination of the H−Xe cross-relaxation rates requires the value of the ^{129}Xe polarization enhancement (see eq 13). $f^{obs}_{Xe}(0)$ is estimated from the quantitative comparison of the integrated intensities of the laser-polarized and equilibrium ^{129}Xe NMR spectra. These spectra need to be recorded in very different conditions (e.g., duration and amplitude of the rf observation pulse, receiver gain, etc.), and the estimation of $f^{obs}_{Xe}(0)$ may be prone to errors. In the present case, broadening of the ^{129}Xe NMR signals originating from exchange (yielding line widths greater than 500 Hz) and the long ^{129}Xe relaxation times (estimated to be in the range of 50 to 90 s in the samples used for SPINOE experiments) are responsible for low signal-to-noise ratios in the equilibrium spectrum. From the experimental data given in Table 1, and using a $f^{obs}_{Xe}(0)$ value measured to be $\sim 1.3 \times 10^4$ (with uncertainty on the order of 50%), σ_{HXe}/A_{129} was estimated to be $\sim 1.2 \times 10^{-4}$ s^{-1} for the aromatic protons (see eqs 13 and 11). From multiple experiments, σ_{HXe}/A_{129} values in the range $1-4 \times 10^{-4}$ s^{-1} were found for the aromatic protons. This figure is 2 orders of magnitude larger than the value expected for H−Xe cross-relaxation rates originating from diffusive coupling; the observed SPINOE enhancements can therefore be considered as originating entirely from the binding of xenon. Furthermore, the SPINOE spectra were obtained with dissolved xenon in excess with respect to the cryptophane-A concentration. Under these circumstances eq 10c is valid, and we have $\sigma_{HXe}/A_{129} = \sigma^b_{HXe}$ (see eq 11).

The largest σ^b_{HXe} values characterizing the binding of xenon to cryptophane-A are found to be significantly smaller (5 to 10-fold) than the largest values observed when xenon binds to α-cyclodextrin.[26] Such a discrepancy is unlikely to originate from differences in the dynamics of the ^{129}Xe → ^{1}H polarization transfer. Indeed, we have shown that for the binding of xenon to cryptophane-A in $(CDCl_2)_2$ at room temperature, σ^b_{HXe} is expected to reach 70% of its maximum value. Instead, the discrepancy in the σ^b_{HXe} values suggests differences in the structure of these xenon complexes. Given $\tau^b_c = 0.6$ ns and $\sigma^b_{HXe} \approx 1-4 \times 10^{-4}$ s^{-1}, eq 4 leads to a $\langle r^{-6}_{HXe}\rangle^b$ value in the range $(0.5-2) \times 10^{-4}$ Å^{-6}; thus, the average distance between the aromatic protons and the xenon atom is 4.1−5.2 Å. These results are in good agreement with computer modeling which gives values of 4.5−4.8 Å (from minimum energy structures of xenon included in the cavity of cryptophane-A, see below). On the basis of an X-ray structure of α-cyclodextrin,[68] the r_{HXe} values between a xenon atom positioned at the center of the cavity and the nearest protons are found to be in the range of 3.2−3.8 Å. These calculated ranges of proton-to-xenon distances translate into a 4- to 8-fold factor increase in the cross-relaxation rates (neglecting dynamical effects), in agreement with the experimental observations.

IV. 4. Relative Values and Structure of the Complex. In section IV. 3. it was shown that the observed SPINOE enhancement for the aromatic protons is consistent with xenon included in the cavity of cryptophane-A. Detailed information

(68) Saenger, W.; Noltenmeyer, M. *Angew. Chem., Int. Ed. Engl.* **1974**, *13*, 552−553.

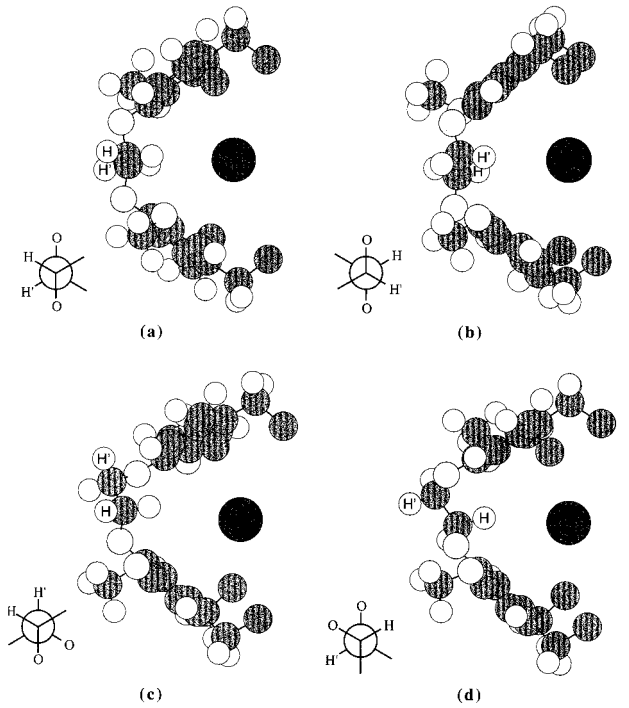

Figure 11. Minimum energy structures of cryptophane-A with included xenon for the various conformations of the displayed spacer bridge. The atoms of the cyclotriveratrylene subunits are at similar positions in each view; the molecule is slightly rotated such that the spacer bridge is clearly visible. In a and b, the linkers are in an anti conformation. In c and d, the linkers are in a gauche conformation.

regarding the structure of the complex can be obtained in the absence of information about the absolute values of σ^{b}_{HXe}; furthermore, the use of relative H−Xe cross-relaxation rates avoids the uncertainty attached to the determination of $f^{obs}_{Xe}(0)$. Table 1 gives the σ^{b}_{HXe} values of the cryptophane-A protons relative to the value for the aromatic protons. From these data it is clear that the binding of xenon to cryptophane-A gives rise to selective $^{1}H-^{129}Xe$ dipole−dipole interactions. Provided that internal dynamics do not contribute significantly to the fluctuations of the intermolecular dipole−dipole interactions, the relative σ^{b}_{HXe} values listed in Table 1 reveal structural information regarding the xenon/cryptophane-A complex. Particularly interesting are the results obtained for the protons belonging to the OCH_2CH_2O spacer bridges (also referred to as linkers). Indeed, one pair of these protons (labeled H_k and $H_{k'}$ in the spectrum in Figure 10b) experiences, in the presence of xenon, a cross-relaxation rate more than twice as large as that between xenon and the other pair of protons (H_j and $H_{j'}$). Because the dynamics of both pairs of protons are most likely similar, these results indicate that H_k and $H_{k'}$ are, on the average, closer to the xenon atom than H_j and $H_{j'}$.

Cryptophane-A belongs to the group of D_3 symmetry. It possesses high intramolecular connectivity and three short spacer bridges linking the two cyclotriveratrylene subunits and is therefore a somewhat rigid molecule. However, the internal degrees of freedom associated with the spacer bridges allow the molecule to adopt various conformations. These conformations involve changes in the dihedral angle $O-CH_2-CH_2-O$ and, referring to the oxygen atoms, are either gauche-like or anti-like in nature. Computer modeling was used to generate minimum energy structures of cryptophane-A with included xenon. Structures are shown in Figure 11 for the various conformations of the displayed spacer bridge. In Figures 11a and 11b, the linkers are in an anti conformation. These

Table 2. Experimental H−Xe Cross-Relaxation Rates (bold) for the Protons of the Spacer Bridges of Cryptophane-A Relative to the Value for the Aromatic Protons and Relative $\langle r^{-6}_{HXe}\rangle^{b}$ Values Calculated Using the Structures in Figure 11 (see text)

	proximal H's	remote H's
experimental	**1.55**	**0.67**
anti 11a	5.2	0.5
anti 11b	4.4	0.5
gauche 11c	1.8	0.3
gauche 11d	1.5	0.3

conformations possess C_2 symmetry axes which bisect the C−C bond of the linkers and intercept at the center of the cavity where the xenon atom is found. Therefore, in Figure 11a the protons labeled H and H′ have the same chemical shift which, a priori, is different from the chemical shift of the other pair of protons. The structures shown in Figure 11b−d were obtained from the structure in 11a, where the labels were left unchanged; the H and H′ which were remote with respect to the xenon atom in Figure 11a are the proximal ones in Figure 11b. In both of these anti conformations the proton−xenon distances are similar and lead to similar relative $\langle r^{-6}_{HXe}\rangle^{b}$ values. From Table 2 it can be seen that the calculated values for the proximal H's in the anti conformations are significantly different from the corresponding experimental result. Even if it were considered that both anti structures are present simultaneously, the experimental results could not be explained. In Figure 11c and d, the linkers are in a gauche conformation. These structures do not possess C_2 symmetry axes, but for each of them an equivalent structure exists in which the position of protons H and H′ are interchanged. Therefore, for each pair of protons, must be calculated as the average between the two protons. It is worth noting that in both of these gauche structures, the partner of the proton which is the nearest to xenon is the farthest proton; in Table 2, this pair is referred to as the "proximal" H's because it leads to the largest $\langle r^{-6}_{HXe}\rangle^{b}$ value. Thus the H and H′ which are "remote" with respect to the xenon atom in Figure 11c become the "proximal" H's in Figure 11d. From Table 2, it can be seen that both gauche structures lead to relative $\langle r^{-6}_{HXe}\rangle^{b}$ values in good agreement with the experimental results. Both of these gauche structures might be present simultaneously, but if this is the case, one conformation must be in considerable excess in order to explain the observed difference in cross-relaxation rates between the proton pairs.

In the last column of Table 1 are listed the relative $\langle r^{-6}_{HXe}\rangle^{b}$ values for the various protons of cryptophane-A calculated using the gauche structures. For the methoxy group, the calculation was carried out for various positions of these protons; the calculation leads to values in agreement with the experimental relative cross-relaxation rates despite the fact that the dynamics of the polarization transfer might be somewhat different in this case. A more rigorous treatment of the expected cross-relaxation rates could be performed using molecular dynamics simulations, and in such calculations the three spacer bridges of cryptophane-A should not be considered independently. Furthermore, our calculations neglect the effects of relayed SPINOEs, which in the present system might be on the order of 10−15% between geminal protons (for a detailed explanation of relayed SPINOEs, see the Appendix). Despite these simplifications, we can conclude on the basis of the experimental SPINOE enhancements that the most probable conformation of the spacer bridges of cryptophane-A when the molecule complexes xenon (in $(CDCl_2)_2$ at room temperature) is a gauche conformation. This conclusion is in agreement with the simulation of resolution-enhanced ^{1}H NMR signals performed elsewhere.[48] Additionally,

we can conclude that the chemical shifts of $H_{k,k'}$ and $H_{j,j'}$ characterize the protons of the spacer bridges of cryptophane-A which are, respectively, gauche and anti with respect to the vicinal oxygen atom.

Conclusion

In this paper a general theoretical framework is given, describing the use of polarization transfer experiments with laser-polarized ^{129}Xe for probing the environment of xenon atoms in solution. The technique was applied to investigate the environment of xenon trapped by cryptophane-A. Selective ^{1}H enhancements were observed, permitting the preferred conformations adopted by cryptophane-A to be determined, and a more complete assignment of the ^{1}H spectrum to be obtained. By using laser-polarized xenon and SPINOE experiments, detailed microscopic information can be obtained, demonstrating the utility of such methods to directly probe molecular structure and dynamics in solution.

Acknowledgment. The authors wish to thank Professor A. Collet and his research group for generously providing samples of cryptophane-A and Tom Lawhead for his expert glass-blowing and advice. M.L. thanks Professor J. Reisse, Dr. J.-P. Dutasta and Dr. K. Bartik for valuable discussions and gratefully acknowledges the Fonds National de la Recherche Scientifique (FNRS, Belgium) for providing financial support. B.M.G. gratefully acknowledges Eastman Chemical for a predoctoral fellowship. D.D.L. gratefully acknowledges the Howard Hughes Medical Institute for a predoctoral fellowship. This work was supported by the Director, Office of Energy Research, Office of Basic Energy Sciences, Materials Sciences Division of the U.S. Department of Energy under Contract DE-AC03-76SF00098.

Appendix

A Three-Spin Model for ^{129}Xe → ^{1}H Polarization Transfer. Consider an isolated three-spin system comprised of two dipolar-coupled protons H_a and H_b, and one ^{129}Xe that interacts with only one of the protons (for example, H_a, with cross-relaxation rate σ_{HXe}). The weak ^{129}Xe−^1H_a dipole−dipole interaction is not considered to contribute to the auto-relaxation rate of H_a. Therefore, both H_a and H_b have the same auto-relaxation rate, ρ, which is solely a consequence of ^{1}H−^{1}H dipole−dipole interactions, and σ is the ^{1}H−^{1}H cross-relaxation rate. Finally, the auto-relaxation of ^{129}Xe is considered to be much slower than the ^{1}H relaxation ($\rho_{Xe} \ll \rho$). The Solomon equations (A1) describe the time dependence of the polarization of the protons H_a and H_b

$$\frac{df_{Ha}(t)}{dt} = -\rho f_{Ha}(t) - \sigma f_{Hb}(t) - \sigma_{HXe}\frac{\gamma_{Xe}}{\gamma_H} f_{Xe}(0) \quad \text{(A1.a)}$$

$$\frac{df_{Hb}(t)}{dt} = -\rho f_{Hb}(t) - \sigma f_{Ha}(t) \quad \text{(A1.b)}$$

where $f_{Ha}(t)$ is the fractional enhancement of the proton H_a (and similarly for H_b and Xe) and γ_{Xe}/γ_H is the ratio of the xenon and proton gyromagnetic ratios. The solution for constant Xe polarization is given by the following relationships:

$$f_{Ha}(t) = e^{-\rho t}[\cosh(\sigma t) f_{Ha}(0) - \sinh(\sigma t) f_{Hb}(0)] - \frac{\gamma_{Xe}}{\gamma_H} f_{Xe}(0) \frac{\sigma_{HXe}}{\rho(1-\eta^2)}[(1 - e^{-\rho t}\cosh(\sigma t)) - \eta e^{-\rho t}\sinh(\sigma t)] \quad \text{(A2)}$$

$$f_{Hb}(t) = e^{-\rho t}[\cosh(\sigma t) f_{Hb}(0) - \sinh(\sigma t) f_{Ha}(0)] - \frac{\gamma_{Xe}}{\gamma_H} f_{Xe}(0) \frac{\sigma_{HXe}}{\rho(1-\eta^2)}[-\eta(1 - e^{-\rho t}\cosh(\sigma t)) + e^{-\rho t}\sinh(\sigma t)] \quad \text{(A3)}$$

where $\eta = \sigma/\rho$, and the H−Xe cross-relaxation rate is defined in section II. 3. (see eq 4). Assuming an exponential decay for the ^{1}H−^{1}H dipole−dipole interaction correlation function, the ^{1}H−^{1}H auto- and cross-relaxation rates are respectively given by[52]

$$\rho = \left(\frac{\mu_o}{4\pi}\right)^2 \frac{\hbar^2\gamma_H^4}{10}\left\langle\frac{1}{r_{HH}^6}\right\rangle[6J(2\omega_H) + 3J(\omega_H) + J(0)] \quad \text{(A4.a)}$$

$$\sigma = \left(\frac{\mu_o}{4\pi}\right)^2 \frac{\hbar^2\gamma_H^4}{10}\left\langle\frac{1}{r_{HH}^6}\right\rangle[6J(2\omega_H) - J(0)] \quad \text{(A4.b)}$$

As expected, the present three-spin model indicates that dipole−dipole interactions between Xe and H_a affect the polarization of both H_a and H_b. Hereafter, the SPINOE for the ^{1}H coupled

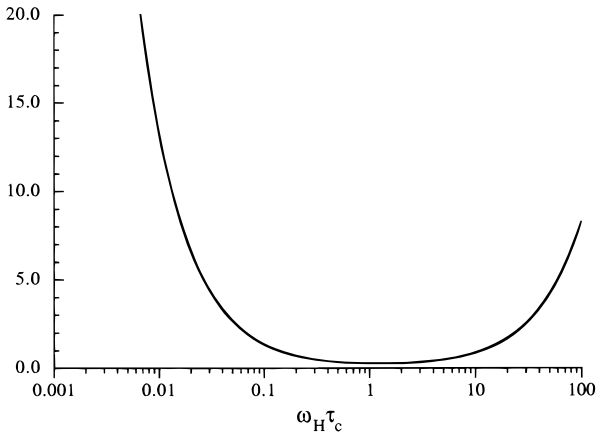

Figure 12. Dependence of $1/\rho(1-\eta^2)$ on the correlation time. The following ratio is displayed: $1/\omega_H[6J(2\omega_H) + 3J(\omega_H) + J(0)](1-\eta^2)$ where $\eta = [6J(2\omega_H) - J(0)]/[6J(2\omega_H) + 3J(\omega_H) + J(0)]$.

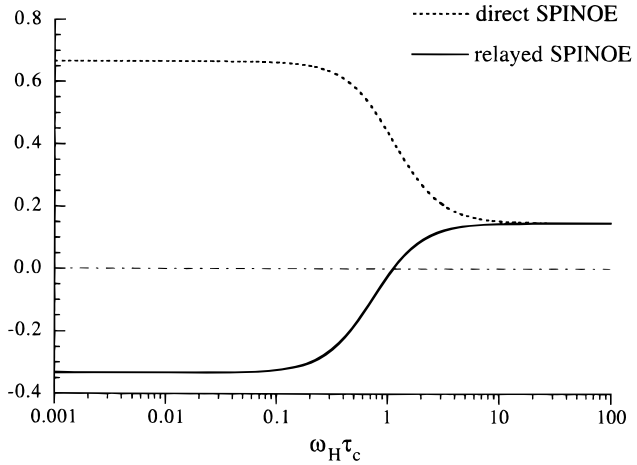

Figure 13. Dependence of maximum ^{129}Xe−^{1}H direct SPINOE (dotted line) and relayed SPINOE (solid line) on the correlation time. The following ratios are displayed: direct SPINOE: $[6J(\omega_H + \omega_{Xe}) - J(\omega_H - \omega_{Xe})]/[6J(2\omega_H) + 3J(\omega_H) + J(0)](1-\eta^2)$; relayed SPINOE: $-\eta \times$ direct SPINOE, with η as defined in the legend of Figure 12.

with ^{129}Xe is referred to as a direct SPINOE, and the SPINOE for the ^{1}H not coupled with ^{129}Xe is referred to as a relayed SPINOE.

Equation A2 indicates that the maximum Xe−H direct SPINOE is given by

$$[f_I(t)]_{\mathrm{d}}^{\max} = -\frac{\gamma_{\mathrm{Xe}}}{\gamma_{\mathrm{H}}} f_{\mathrm{Xe}}(0) \frac{\sigma_{\mathrm{HXe}}}{\rho(1-\eta^2)} \qquad \text{(A5)}$$

The dependence of σ_{HXe} on the correlation time is shown in Figure 3 (section II). The dependences of $1/\rho(1-\eta^2)$ and $\sigma_{\mathrm{HXe}}/\rho(1-\eta^2)$ on τ_c are shown in Figures 12 and 13, respectively. The dependence depicted in Figure 13 applies for direct SPINOE originating from xenon binding; under such circumstances, the fluctuations of both the ^{129}Xe−^{1}H and ^{1}H−^{1}H dipole−dipole interactions are characterized by a single correlation time. Even though σ_{HXe} increases by a ∼20-fold factor for increasing $\omega_{\mathrm{H}}\tau_c$ values in the range 0.01−0.68 (see Figure 3, section II), the direct SPINOE is essentially constant, then decreasing. For diffusive coupling, it is worth noting that the dynamics of σ_{HXe} are not expected to change significantly with increasing solute size (at least in dilute solutions) and therefore the direct SPINOE goes as $1/\rho(1-\eta^2)$, as depicted in Figure 12. Clearly, the importance of the direct SPINOE due to diffusive coupling decreases for increasing solute size.

Equation A3 indicates that the maximum Xe−H relayed SPINOE is given by

$$[f_I(t)]_{\mathrm{r}}^{\max} = -\frac{\gamma_{\mathrm{Xe}}}{\gamma_{\mathrm{H}}} f_{\mathrm{Xe}}(0) \frac{-\sigma_{\mathrm{HXe}}\eta}{\rho(1-\eta^2)} \qquad \text{(A6)}$$

The importance of the relayed SPINOE relative to the direct SPINOE is thus equal to $-\eta$. The dependence of $-\sigma_{\mathrm{HXe}}\eta/\rho(1-\eta^2)$ on the correlation time is shown in Figure 13. For positive $f_{\mathrm{Xe}}(0)$ values and short correlation times, negative relayed SPINOEs are expected, whereas positive direct SPINOEs would be observed under these conditions.

JA9841916